Study of the Local Multipoint Distribution Service Radio Channel

Peter B. Papazian, George A. Hufford, Robert J. Achatz, Randy Hoffman
National Telecommunications and Information Administration
Institute for Telecommunication Sciences
325 Broadway, Boulder, CO 80303

Abstract. This paper summarizes radiowave propagation impairments for local multipoint distribution services (LMDS) and reports measurement data for small cells. Results include area coverage estimates over a range of basic transmission losses for 0.5-, 1.0- and 2.0-km suburban cells with foliated trees. Multipath, signal attenuation, depolarization, and cell to cell coverage also are discussed. Data indicates a high probability of non-line-of-sight paths due to trees which can cause signal attenuation and signal variability when wind is present. Signal variability was studied using k factors and compared to the Rician cumulative distribution function. Depolarization caused by vegetation and other signal scatterers was found to be an order of magnitude greater than rain-induced depolarization. A simple tapped delay line model is presented to describe multipath for three channel states.

Introduction

Millimeter wave communication systems in the 27.5 to 29.5 GHz band are being developed in the United States and Canada for use in a local multipoint distribution service (LMDS). It is envisioned that these systems could broadcast voice, video, and data, and would allow for interactive communications in small cells. To compete successfully with standard broadcasting, cable, and satellites, the signal would need to be reliable and of high quality. Critical propagation issues are clear-air absorption, signal attenuation by rain, vegetation and buildings, signal depolarization, multipath, and cell-to-cell interference. An initial study of the radio channel for a suburban neighborhood with defoliated trees was made by Papazian, Roadifer, and Hufford [1]. Clear-air absorption at millimeter-wave frequencies has been modeled by Liebe [2,3]. Summary results, applicable to LMDS propagation, for clear air absorption, attenuation, and depolarization by rain have been reported by Dalke and Hufford [4]. This study quantifies area coverage, attenuation by vegetation, depolarization, and multipath for two suburban neighborhoods with foliated trees. A method for determining area coverage is presented and coverage estimates are made for several cell sizes and two transmitter heights.

Equipment

Measurements were made using a radio channel probe configured to transmit a 28.8-GHz narrowband continuous wave (CW) signal and a 30.3-GHz wideband signal through a common traveling wave tube amplifier. These signals were received using a parabolic dish antenna, and then split, down converted and processed in separate receivers. The narrowband signal is band pass filtered with a 2-kHz filter and then detected using a log amplifier. The narrowband receiver has a sensitivity of -130 dBm and a dynamic range of 70 dB. The wideband transmitter uses a 500-Mb/s pseudo-random noise code to modulate the carrier. Its receiver is a sliding correlator that uses a duplicate pseudo noise generator. The correlator produces co-phase and quadrature-phase impulse response data with 2 ns resolution. The wideband receiver has a sensitivity of -102 dBm and a dynamic range of 50 dB.

We used a vertically polarized horn transmit antenna with 14 dB gain. The horn antenna has a 90° azimuthal 3 dB beamwidth, and a 20° vertical beamwidth. Equivalent isotropically radiated power for the transmitter was 51 dBm. The receiver antenna system consisted of two 2.5° dishes with linearly polarized feeds. One dish was aligned for vertical polarization and the second was aligned for horizontal polarization. The signal was routed to the receiver using waveguides with a switch to select the vertically or horizontally polarized antenna. These antennas and the receiver were mounted on a 28-ft pneumatic mast fitted with a pan-tilt head to control the azimuth and elevation angle.

Survey Sites

Suburban areas in Northglenn, Colorado and in San Jose, California were surveyed. Both sites consist predominantly of one- and two-story single family residences which are about 30 years old. Both areas have small yearly rainfall totals and slow tree growth. Some relevant geographic statistics for each site are listed in Table 1.

Table 1. House density, normal temperature, and rainfall averages for Northglenn, Colorado and San Jose, California.

Geographic Statistics	Northglenn, Colorado	San Jose, California
Number of houses / km^2	780	900
* Temperature (°F)	50.3	59.7
** Precipitation (in)	15.31	13.86

* Monthly Average.
** Yearly normal between 1951-1980.

Factors that can affect coverage at our sites include terrain, shadowing by buildings and attenuation by vegetation.

The terrain at both survey sites is flat. This removes terrain as a factor when comparing results from Northglenn, Colorado and San Jose, California. In San Jose, the site was bordered to the west by the Santa Teresa Hills, which enabled a second transmitter site to be elevated by an additional 40 ft.

The distributions of roof heights for each site were estimated from measured data. Because these distributions were similar for both sites, shadowing by buildings could not be used to explain differences in the coverage results between the sites.

The most important difference between the sites is the vegetation, in particular the tree canopy. The tree population in Northglenn, Colorado is dominated by elms, maples, cottonwoods and ponderosa pines. Mature trees of these species are 30 to 50-ft tall. In contrast, many trees in San Jose have tropical origins. This causes them to be killed periodically due to sporadic frosts. Consequently, the trees in San Jose are not as mature as in Northglenn. In addition, San Jose has less space for growth, and increased pruning has led to a lower and less dense tree canopy than in Northglenn.

The objectives for Northglenn, Colorado were to quantify area coverage, short term time variations of the signal power, multipath, signal depolarization, and cell-to-cell coverage. We used 40-ft high transmitter sites arranged on a 1.0-km grid. This spacing produced 0.5-km square cell quadrants.

In San Jose area coverage measurements were repeated for a 0.5-km square cell quadrant. We also extended area coverage estimates to larger cells of 1-km and 2-km radii and investigated the area coverage dependence on transmitter height.

Data Collection

In Northglenn, both narrowband and wideband data were collected. The narrowband data includes a time series record of the signal power which was used to study area coverage, short term time variations of the signal, depolarization and cell-to cell coverage. This data was recorded at 1 kilosample/second (ks/s) for 50 s. Wideband data, which was used to study multipath, consists of 100 complex impulse responses at each measurement site. Each impulse lasts for 254 ns and is sampled 1000 times. The repetition rate of the impulses from the sliding correlator is 10 Hz. Both data sets were collected using vertical (co-polarized) and horizontal (cross-polarized) receive antennas at two heights.

In San Jose, only narrowband data were collected using a vertically polarized receiving antenna at one height. This data also was collected at a rate of 1 ks/s for 50 s. The transmit antenna was the same vertically polarized horn used in Northglenn.

Measurement Procedures

The receiver address was determined by randomly selecting houses using aerial photographs of the survey area. Because it was assumed that the probability of acceptable coverage would decrease with distance, each cell was first subdivided into bands of increasing radii from the transmitter. Stations (houses) were then selected randomly from equal area subdivisions of each band. The number of stations needed for an acceptable error was determined by assuming that the area coverage estimate could be modeled using a binomial distribution. Figure 1 shows the 0.5-km square cell with its three sampling bands. Figure 2 shows the 1-km cell, which is circular and has two sampling bands. The 2-km cell is also circular with three sampling bands. Band I for this cell is 500-m wide, band II is 500-m wide and band III is 1000-m wide.

At each station the curbside location of the measurement van was selected using both aerial photographs and onsite inspection to avoid obvious obstructions between the roof of the house and the transmit antenna. The receive antenna height was determined by using a mast-mounted video camera to locate the height of the roof peak above street level and then by raising the mast an additional meter. If a second receive antenna elevation was needed the mast was positioned 2 m above the roof peak. The optimum antenna azimuth and elevation angle then were determined using narrowband, vertically polarized azimuth and elevation scans at each antenna height.

In Northglenn and San Jose it was desired to

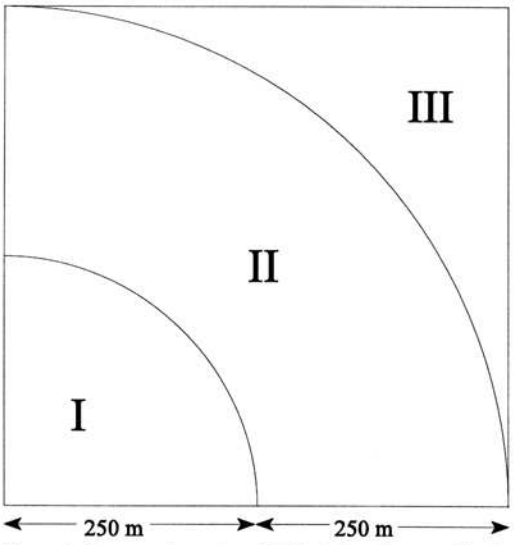

Figure 1. Square cell quadrant (0.5 km) showing sampling bands I, II and III used in Northglenn, Colorado and San Jose, California.

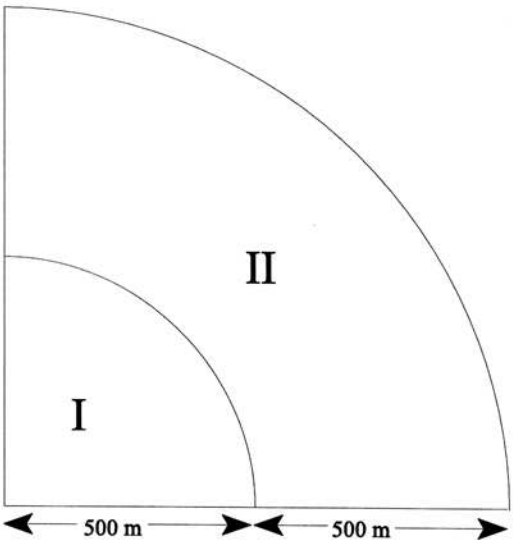

Figure 2 - 1 km circular cell quadrant showing sampling bands I and II in San Jose, California.

estimate coverage for cells that could be separated into four symmetric quadrants. To save time, only one quadrant of each cell was sampled. It was assumed that the other quadrants would be sufficiently uniform and would produce similar results for the entire cell. In Northglenn, two 0.5-km square cell quadrants were surveyed using different 40-ft high transmitter locations and the area coverage results compared. In San Jose one 0.5-km square cell quadrant and a 1-km circular cell quadrant were surveyed using a 40-ft high transmitter site. To study the area coverage dependence on transmitter height an 80-ft high transmitter site was used and the 0.5-km quadrant and 1-km quadrant were resurveyed and a 2-km circular cell quadrant was added.

Area Coverage Model

Area coverage estimates were based on narrowband received power data collected using the copolarized receive antenna. Using this power data, area coverage in each cell band can be estimated as the fraction of houses for which an adequate signal is available for a given percentage of the time. If p_i is the area coverage probability for the band, n_i is the number of houses sampled and n_{il} is the number of houses in the i^{th} band that meet the signal level requirements for coverage, the area coverage estimate is

$$p_i = \frac{n_{il}}{n_i} .$$

Assuming that the area is sampled without replacement, the standard error σ_i in each cell band can be approximated as [5]

$$\sigma_i = \sqrt{p_i(1-p_i)\left(\frac{1}{n_i}-\frac{1}{N_i}\right)} ,$$

where N_i is the number of houses in the i^{th} band. The area coverage p_c and error estimates σ_c for each cell are calculated by weighting the results from each band using their relative area a_i and summing with the following equations:

$$p_c = \sum_{i=1}^{j} a_i p_i$$

$$\sigma_c = \sqrt{\sum_{i=1}^{j} a_i^2 \sigma_i^2} .$$

Radio Channel Characteristics

Basic transmission loss L_b is the signal loss expected between ideal, loss-free, isotropic transmitting and receiving antennae [6]. This loss is a function of the frequency, path length, and attenuation on the path. Attenuation can be caused by atmospheric gases, water vapor, precipitation and other obstructions that cause scattering, absorption, and diffraction of the radio signal. The major source of attenuation for our survey was obstruction of the radio path by buildings and vegetation. Since L_b can

be used to determine available signal power at the receive site, it is used to quantify our area coverage results. A station has coverage if $L_b \leq L_b^{max}$. By using the cumulative distribution function (CDF) of the power, the signal variation at each receiving station, and hence L_b as a function of availability, can be studied. For instance, the median signal power gives L_b for 50 % availability while the lower decile gives L_b for 90% availability. Using L_b calculated at specific availability levels and the statistical development of the previous section, area coverage and standard error estimates are made for a range of L_b^{max}. An area coverage estimate for three availability levels is shown for one of the 40-ft Northglenn transmitter sites in Figure 3. As expected, coverage decreases at increased availability levels. Because a high level of availability is desirable we have summarized area coverage results versus L_b^{max} using 99% availability for all our sites, cells, and transmitter heights. For coverage estimates at higher availability levels more independent power samples would be required.

Area coverage results for the two 0.5-km cell quadrants in Northglenn, Colorado (T1 and T3) are compared in Figure 4. We see area coverage ranges from 20 to 70% and could be described using a linear best fit curve. Figure 5 gives results for a similar 0.5-km cell quadrant and a 1.0-km cell quadrant, both using a 40-ft high transmitter site in San Jose, California. In San Jose, the probability of coverage for the 0.5-km cell increases by about 0.3 for L_b of 135 dB relative to Northglenn. The two coverage curves converge to within 0.1 unit as the L_b bound is raised to 155 dB. As previously stated, these coverage variations are presumed related to difference in the tree canopy at each site. Also shown in Figure 5 are results for the 1-km cell which are offset by -0.3 to -0.5 probability units from the 0.5-km square cell results. In Figure 6, we see that the area coverage for San Jose is improved significantly for the 0.5 and 1-km cells by using an 80-ft high transmitter site. For the 2-km cell using the 80-ft site, probability of coverage drops to 0.2 for L_b^{max} of 135 dB and then increases linearly to 0.65 for an L_b^{max} of 155 dB.

Attenuation

It is convenient to separate L_b into its two components, attenuation A and basic free space loss L_{bf},

$$L_b(dB) = L_{bf}(dB) + A(dB).$$

Using this relationship A is calculated by subtracting L_{bf} from L_b where L_{bf} is [6]

$$L_{bf}(dB) = 32.4 + 20\log f\,(MHz) \cdot d(km)\ .$$

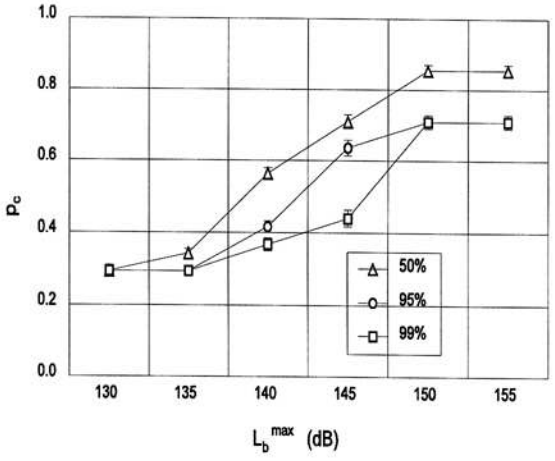

Figure 3. Area coverage probability estimate p_c versus L_b^{max} for 50%, 95% and 99% availability levels for cell T1 in Northglenn, Colorado.

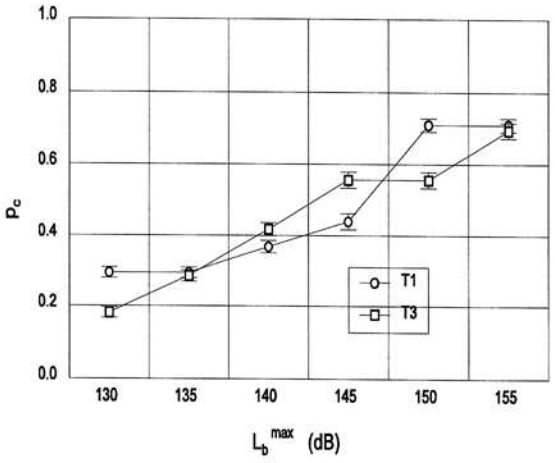

Figure 4. Area coverage probability estimate p_c versus L_b^{max} for 99% availability for cells T1 and T3 in Northglenn, Colorado.

An attenuation versus distance graph for San Jose using the 40-ft transmitter site is shown in Figure 7. The data is highly scattered due to the random nature of the obstructions. However, a general trend can be seen by overlaying a linear least squares fit curve on the data. Similar linear fits were made using the other Northglenn and San Jose data. The slopes and intercepts of these curves are summarized in Table 2.

The slope of the attenuation data has an expected inverse correlation with the area coverage results. Northglenn, which had the smallest coverage estimate, has the largest attenuation slope. Coverage increased slightly in San Jose for the 40 ft transmitter site and the attenuation slope was smaller. The attenuation slope decreased

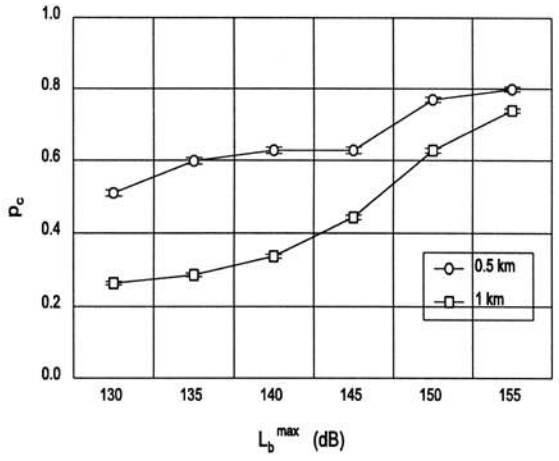

Figure 5. Area coverage estimate p_c versus L_b^{max} at 99% availability for 0.5 km and 1.0 km cells using a 40-ft transmitter, San Jose, California.

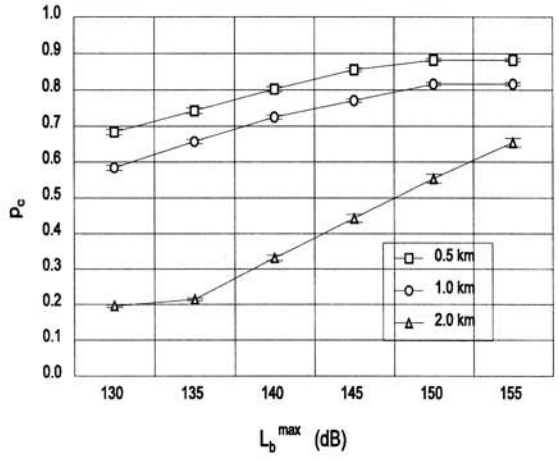

Figure 6. Area coverage probability estimate p_c versus L_b^{max} at 99% availability for 0.5, 1.0 and 2.0 km cells using the 80-ft transmitter, San Jose, California.

significantly when the 80 ft transmitter site was used in San Jose indicating that the radio path was able to clear many more obstructions. When a tree is blocking the radio path, signal propagation will be dependent on scattering and diffraction. In many cases when a tree was obstructing the radio path it was located within 10 to 20 m of the receiver site. For the 500-m cell, using an average path length of 250 meters and the obstruction placed at 235 m, the diameter of the first Fresnel zone for a 30 GHz signal is about 1 m. Usually line of site radio links require 60% of the first Fresnel zone to be free of obstructions to limit diffraction losses. Using this criteria would require a 77 cm clearance hole through the tree canopy for an unobstructed radio path with minimal diffraction loss caused by the canopy.

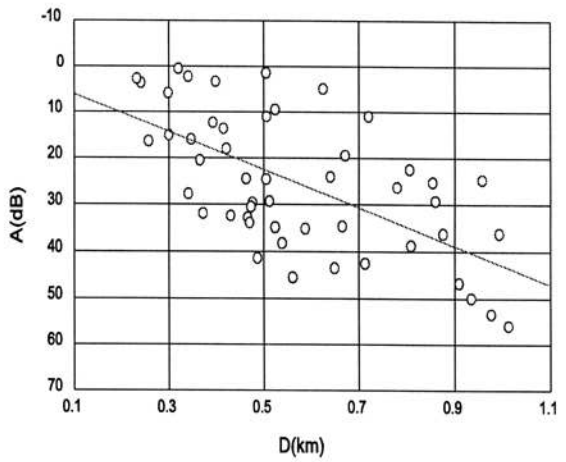

Figure 7. Attenuation versus distance using the 40-ft transmitter , San Jose, California.

Table 2. - Attenuation versus distance slope and intercept data for Northglenn, Colorado and San Jose, California.

Site	Slope (dB/km)	Intercept (dB)
Northglenn,(40-ft transmitter)	42.4	7.3
San Jose, (40-ft transmitter)	40.9	2.1
San Jose, (80-ft transmitter)	6.7	9.4

In addition to arguments using Fresnel diffraction zones, large signal attenuation by trees is consistent with previous experiments conducted by The Institute for Telecommunications Sciences (ITS) which were used to characterize millimeter-wave propagation in vegetation [7,8,9,10]. Measurements in regularly planted orchards have found attenuation values between 12-20 dB per tree for 1 to 3 deciduous trees and up to 40 dB for 1 to 3 coniferous trees. Our measured ranges of attenuation can be accounted for by a combination 1 to 4 coniferous and deciduous trees on the radio path.

Cross-polarization Discrimination

Cross-polarization discrimination measurements were made in Northglenn to test the practicality of frequency reuse schemes that employ signals of orthogonal polarizations. For these measurements, a vertical linearly polarized signal was transmitted and both vertically and horizontally polarized signals were received. The ratio of co-polarized received

power $w_{\parallel}$ to cross-polarized received power $w_{\perp}$ expressed in dB is commonly referred to as the cross-polarization discrimination.

$$XPD = 10 \log \frac{w_{\parallel}}{w_{\perp}} .$$

The larger XPD is the more effective orthogonal frequency reuse will be. At millimeter-wave frequencies, rain-induced depolarization is produced by differential attenuation caused by non-spherical raindrops. Dalke and Hufford [4] presented rain depolarization results at 30 GHz using empirical formulas for oblate spheroidal drops provided by the CCIR [11]. They found that the specific attenuation for horizontally polarized waves at a rain rate of 10 mm/hr is 0.3 dB/km more than for vertically polarized waves. They also presented results for XPD versus rain attenuation at 28 GHz. Again, using empirical relationships from the CCIR [12], XPD remained above 24 dB for rain attenuation up to 30 dB. Of more concern is the depolarization caused by scattering from vegetation. Experiments conducted at the ITS [7,8,9,10] have characterized millimeter-wave depolarization in both coniferous and deciduous orchards. The most serious impairments are seen consistently in conifer tree stands where the average XPD at 28.8 GHz was 12 dB for foliage depths of 20 m and decreased to about 9 dB after 60 m. However, it is difficult to apply these results to cells proposed for LMDS applications because the foliage depth and tree species for any particular subscriber are random and unknown. Measured XPD results for the two Northglenn cells (T1 and T3) are presented as a function of attenuation in Figure 8. The data is highly scattered but a linear fit predicts an XPD of 14 dB at an attenuation of 30 dB which is 10 dB more severe than the XPD predicted due to rain by the CCIR.

Cell-to-Cell Coverage

A small number of cell-to-cell coverage measurements were made in Northglenn by reoccupying four receiver stations which had L_b values larger than 155 dB and using transmitters located in two of four possible adjacent cells. Seven of the eight L_b readings were between 179 and 192 dB and one L_b value was 149 dB. Based on these results increased coverage or interference due to line of sight conditions between cells is minimal for Northglenn.

Radio Signal Description

For modeling purposes, the radio signal is described in two ways. The first uses k factors to analyze short-term time variations of received signal power. The second, represents the radio channel

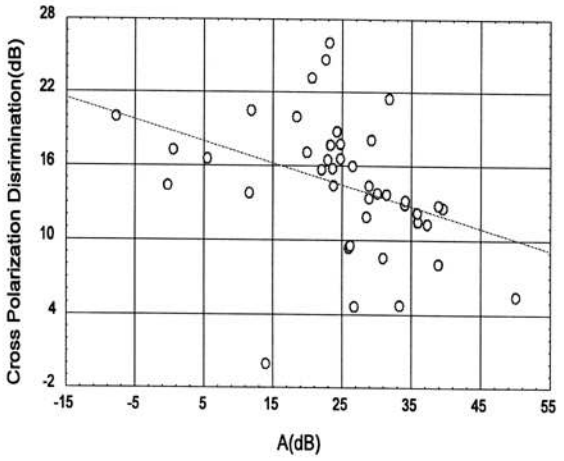

Figure 8. Cross polarization discrimination (XPD) versus attenuation for 0.5 km cells using 40-ft transmitters in Northglenn, Colorado.

impulse response as a tapped delay line with one to three taps.

K Factors

The radio paths that we consider here are short, nominally line-of-sight paths that may be accidentally interrupted by roof tops or trees. One common way to picture the electromagnetic fields at the receiving antenna is as a sum of the wave coming directly from the transmitter, and a multitude of small waves scattered from adjacent houses and from the leaves of nearby trees. Since the phases of the scattered waves will be random, the resulting signals are best treated statistically. The small waves, when represented as complex voltages, will add together algebraically to produce a complex Gaussian process whose amplitude (or instantaneous power) is Rayleigh distributed. When the constant direct wave is included, the resulting amplitude should follow the Nakagami-Rice (or Rician) distribution. This distribution has two parameters which can be chosen in a variety of ways. The first is to use the power w_c in the constant wave and the average power w_s in the scattered wave. Normally, however, one uses the average total power and the ratio $k=w_c/w_s$ of the two components. The ratio is called the k-factor which often is represented in decibels.

In Figure 9 we have plotted the complementary cumulative distribution function for Nakagami-Rice distributions with several different k-factors. For these plots we have used "Rayleigh paper" in which the probability scale has been so constructed that the Rayleigh distribution appears as a straight line with slope -1. Note that the curves in Figure 9 are almost straight lines with shallower slopes. The extreme case with k = 0 is just the Rayleigh distribution while

with k infinite ($w_s = 0$) the distribution degenerates to the unit step function. For convenience all of the curves have been drawn passing through a median power of 0 dB.

Measured data that represent such statistics must be taken somewhat indirectly. Presumably, the median power and k-factor change when we change location, so to obtain a homogeneous sample we must remain in one place. One solution is to move the receiving antenna by a few wavelengths. Presumably this changes the phases of all scattered components and so provides independent data. A second solution is to record the variation in time. Assuming that such variability is due to the wind in the trees (or to traffic moving in the streets) one can again expect the phases to change and perhaps to change enough to provide a suitable sample.

It is, of course, time variability that our narrowband measurements recorded. We have examined each measurement run, assembled the received signal levels, and arrayed them for various computer analyses. Note, for instance, that if the data do follow a Nakagami-Rice distribution, then the mean w (the average power in watts) is simply the total power $w_c + w_s$ while the variance is $2w_c w_s + w_s^2$. Thus, by computing these moments we can solve for both w_c and w_s, and then evaluate k.

In Figure 10 we have plotted several measured cumulative distribution functions. The measurements involved were chosen arbitrarily from the complete list, in order to provide k-factors equal to those in Figure 9. One notes that while the high fields towards the left seem to follow the expected curves, the low fields on the right do not. The fades are not deep enough. This seems to be a real fact; for example, none of the paths involved had fields within 5 dB of the receiver sensitivity at -130 dBm. Our conclusion is that this is an important result and that we must abandon the assumptions that lead to the Nakagami-Rice distributions.

We would suggest that the observed variability is caused by a different mechanism: the direct wave is interrupted by a tree and the tree is not entirely opaque, but has gaps in its foliage that allow some of the energy through. The wind then changes the gaps and the signal varies. Numbers seem to be about right. Suppose the tree is 20 m away from the receiving antenna. The 2.5° beamwidth would collect energy from a circle about 1 m in diameter, and as mentioned before, a Fresnel zone at that distance is also about 1 m across. Unfortunately, such a mechanism does not seem to lead to a natural statistical treatment, although we have had some success representing the data with the log-normal distribution.

Whether or not we accept the assumptions leading to the Nakagami-Rice distribution, the k-factor remains a fairly good measure of the variability of the observed signal. In Figures 11 and 12, we have plotted the computed k-factor versus the observed average attenuation. As the attenuation increases, there does seem to be some increase in the variability, just as one would expect.

The data in Figure 11 were from Northglenn and include both the co-polarized and cross-polarized measurements. There seems to be very little difference in the variabilities of the two sets. Figure 12 shows the data from San Jose and includes both transmitter antenna heights. Here, there does seem to be some difference, with the higher antenna having the greater variability. Perhaps wind conditions changed between the survey days.

Tapped Delay Line Channel Model

The tapped delay line channel model is,

$$h(t) = \sum_{n=1}^{N} \beta_n \, \delta(t-\tau_n) \, e^{-j\omega_c \tau_n} ,$$

where $h(t)$ is the complex channel impulse response, N is the maximum number of taps, n is the tap index, β is the tap gain, τ is the tap delay, and ω_c is the carrier frequency.

We selected three stations located at successively greater distances from the transmitters along the same cell radial to represent good, moderate, and bad wideband channels. Table 3 summarizes the channel model at these stations. The small delay spreads confirm that there are few specular reflections due to the filtering effect of the narrowbeam receiver antennas. We note that delay spread is calculated using a 20 dB threshold. Table 4 lists the distance D between transmitter and receiver, attenuation A, delay spread S and L_b for these paths. From Table 4 we see that links which exhibit multipath also have larger values of L_b and attenuation. Delay spreads S are also plotted versus attenuation in Figure 13. This plot also indicates that multipath is associated with larger signal attenuations. One explanation is that the multipath is caused by multiple scattering events.

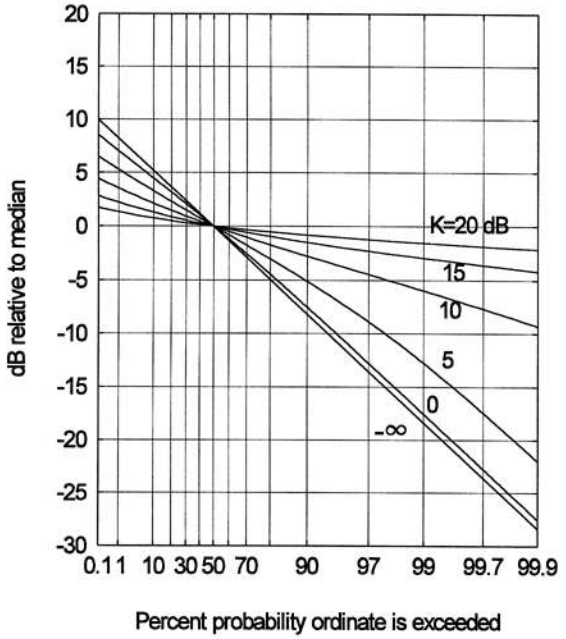

Figure 9. Nakagami-Rice CDF's for various k factors plotted on Rayleigh paper.

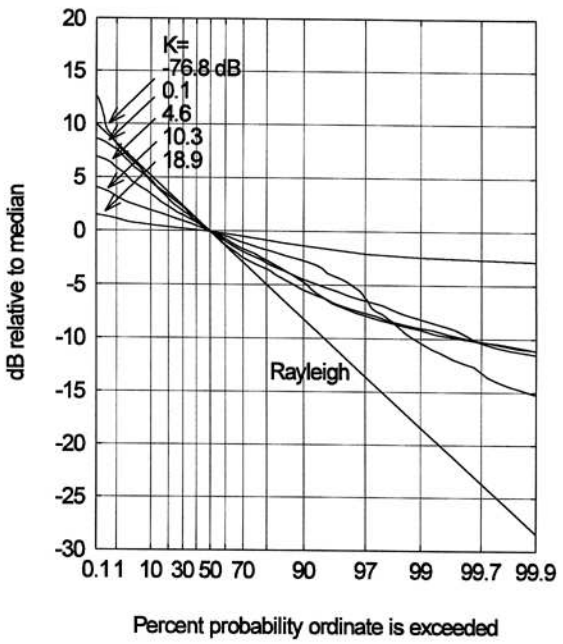

Figure 10. Selected examples of measured data for various k factors plotted on Rayleigh paper.

Table 3. - Summary of tapped delay line models for good, moderate, and bad channels from Northglenn, Colorado.

Quality	Tap #	β_n (dBm)	τ_n (ns)
Good	1	0	0
Moderate	1	0	0
Moderate	2	-13.7	5.3
Bad	1	0	0
Bad	2	-2.8	3.6
Bad	3	-16.2	15.3

Table 4. - Summary of distance D, attenuation A, delay spread S and basic transmission loss L_b at 99 % exceedance for three wideband channels in Northglenn, Colorado.

Quality	D (m)	A (dB)	S(ns)	L_b (dB)
Good	122	6.2	1.26	111.7
Moderate	309	32.2	1.60	145.9
Bad	419	32.6	2.95	159.4

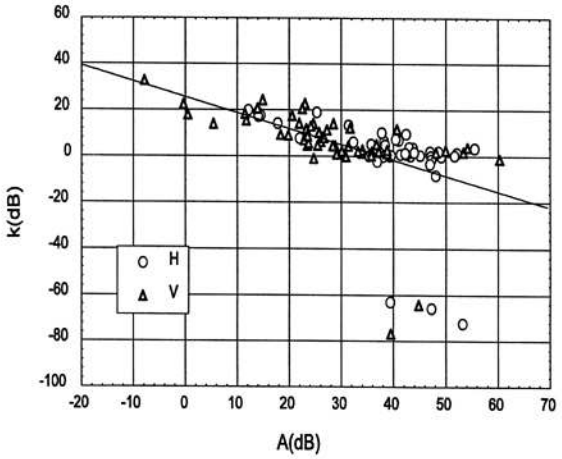

Figure 11. K factors versus attenuation for vertical and horizontal polarization using 40-ft transmitters in Northglenn, Colorado.

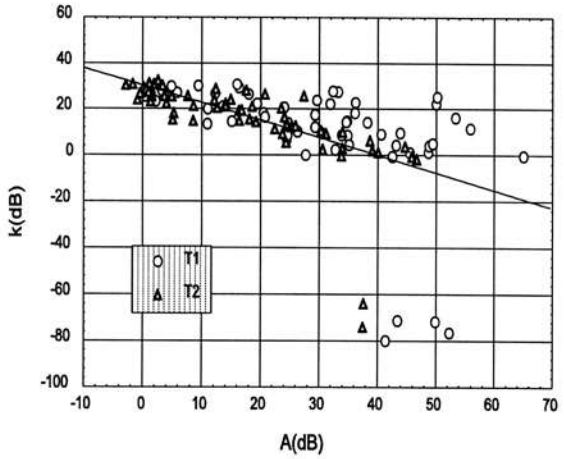

Figure 12. K factors versus attenuation using 40-ft (T1) and 80-ft (T2) transmitters in San Jose, California.

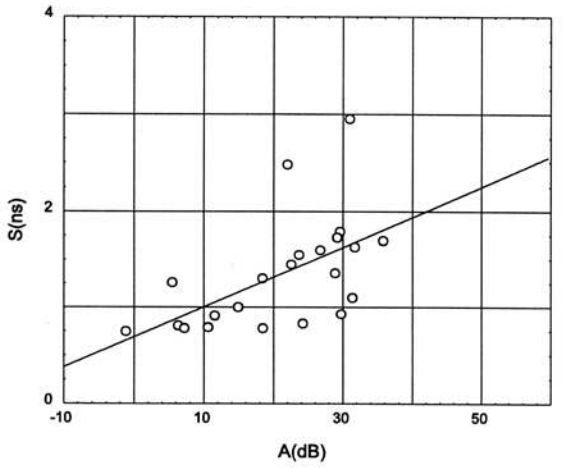

Figure 13. Delay spread (S) versus attenuation, 40-ft transmitters, Northglenn, Colorado.

Conclusions

The most serious propagation impairment for LMDS in the two surveyed suburban neighborhoods was signal attenuation. Attenuation is caused by the tree canopy which extends above roof height. This canopy blocks line-of-sight to the transmitter and can cause signal attenuation, depolarization, and multipath. The primary mode of signal propagation through trees is thought to be diffraction. When diffraction by the tree canopy is combined with wind signal variability results. K factors were found to be a good measure of variability but the Nakagami-Rice distribution predicted deeper fades than were observed. We also found multipath, which is believed to be caused by multiple scattering events instead of multiple specular reflections.

Area coverage estimates for LMDS were found to vary considerably with cell size, transmitter height, and L_b^{max}. For all cells coverage can be increased by relaxing L_b^{max} requirements; however, this will increase multipath and depolarization for the radio channel. These propagation impairments will decrease available channel bandwidth for digital transmission schemes and limit frequency reuse based on orthogonal polarizations.

Acknowledgments

The authors would like to thank the National Telecommunications and Information Administration and the Hewlett Packard Corporation for sponsoring this work through a cooperative research and development agreement.

References

[1] P.B. Papazian, M. Roadifer, G.A. Hufford,"Initial study of the local multipoint distribution system radio channel," NTIA Report 94-315, August 1994.

[2] H.J. Liebe, "MPM an atmospheric millimeter-wave propagation model," *Int. Jour. Infrared and Millimeter Waves*, pp. 631-650, 1989.

[3] H.J. Liebe, G.A. Hufford, and M.G. Cotton, "Propagation modeling of moist air and suspended water/ice particles at frequencies below 1000-GHz," in *Proc. AGARD Conference on Atmospheric Propagation Effects through Natural and Man-Made Obscurants for Visible to MM-Wave Radiation*, 1993, pp. 3-1 to 3-11.

[4] R.A. Dalke, G.A. Hufford, R.L. Ketchum,"Radio propagation considerations for local multipoint distribution systems," NTIA Report 96-331, Aug. 1996.

[5] M. Kendall and A. Stuart, The Advanced Theory of Statistics, Macmillan Pub. Co., New York, 1977.

[6] M.P.M. Hall, Effects of the troposphere on radio communication. *IEE Electromagnetic Wave Series 8,* Peter Peregrinus Ltd., 1979, pp.10-13, pp. 81.

[7] D. Jones, R. Espeland, and E. Violette, "Vegetation loss measurements at 9.6, 28.8, 57.6, and 96.1-GHz through a conifer orchard in Washington state," NTIA Report 89-251, Oct. 1989. (NTIS Order No. PB 90-168717).

[8] E. Violette, R. Espeland, and F. Schwering, "Vegetation loss measurements at 9.6, 28.8, and 57.6-GHz through a pecan orchard in Texas", *Multiple Scattering of Waves in Random Media and Random Rough Surfaces*, State College, PA: Pennsylvania State Univ., 1985, pp. 457- 472.

[9] P.B. Papazian, D. Jones and R. Espeland,

"Millimeter-wave Propagation at 30.3-GHz through a Pecan Orchard in Texas," NTIA 92-287, Sept. 1992.

[10] E. Violette, R. Espeland, and K.C. Allen, "Millimeter-wave propagation characteristics and channel performance for urban-suburban environments," NTIA Report 88-239, Dec. 1988. (NTIS Order No. PB 89-180251/AS).

[11] CCIR, "Attenuation by hydrometeors, in particular precipitation, and other atmospheric particles," *Recommendations and Reports of the XVIIth Plenary Assembly*, Report 721, 1990.

[12] CCIR, "Propagation data and prediction methods required for earth-space telecommunications systems," *Recommendations and Reports of the XVIIth Plenary Assembly*, Report 564, 1990.

Peter B. Papazian (M'91) was born in New York in 1950. He received the B.S. degree in physics from the State University of New York at Stonybrook in 1973, and the M.S. degree in geophysics from the Colorado School of Mines in 1979. His work experience includes electromagnetic modeling and EMC engineering. In 1990 he joined the Radio Research and Standards group at the Institute for Telecommunication Sciences in Boulder, Colorado. His research concerns millimeter-wave propagation, impulse response measurements and man-made radio noise measurements.

George A. Hufford (S'45 A'49 M'55 L'95) was born in San Francisco, California in 1927. He received the B.S. degree in engineering from Cal Tech in 1946, the M.S. degree in electrical engineering from the University of Washington in 1948, and the Ph.D. degree in mathematics from Princeton University in 1953. In 1964 he joined the Department of Commerce as a member of the Tropospheric Telecommunications Laboratory, CRPL, in Boulder, Colorado, and has remained there although his organization has undergone several name changes and is now the Spectrum Division of ITS, NTIA, in the Department of Commerce. In these years he has been active in research related to the computation and modeling of tropospheric radio propagation under real-world conditions as when irregular terrain and a changing atmosphere are involved.

Dr. Hufford is a member of the American Mathematical Society, the Society of Industrial and Applied Mathematics, and Sigma Xi.

Robert James Achatz (S'81 M'84) is an engineer in the Radio Research and Standards group at the Institute for Telecommunication Sciences in Boulder Colorado. He obtained his BSEE and MSEE from the University of Colorado in 1984 and 1993. His current research interests at the Institute are modeling and simulation of radio systems.

J. Randy Hoffman obtained a B.S.(1972) in physical science at Colorado State University, and a B.S.E.E. (1990) from the University of Colorado at Denver. He is a member of the Radio Research and Standards Group at the Institute for Telecommunications Sciences in Boulder, Colorado and has been instrumental in several propagation studies. His work on this project included acquisition software development and field measurements.